HHS Public Access

Author manuscript

Lab Invest. Author manuscript; available in PMC 2013 September 01.

Published in final edited form as:

Lab Invest. 2013 March ; 93(3): 268–278. doi:10.1038/labinvest.2012.179.

Expression of Osteoprotegerin from a Replicating Adenovirus Inhibits the Progression of Prostate Cancer Bone Metastases in a Murine Model

James J. Cody[1,*], **Angel A. Rivera**[2,*,#], **Gray R. Lyons**[1,†], **Sherry W. Yang**[1], **Ming Wang**[2], **Jason W. Ashley**[1], **Sreelatha Meleth**[3,‡], **Xu Feng**[1], **Gene P. Siegal**[1,4,5], and **Joanne T. Douglas**[2,5]

[1]Department of Pathology, The University of Alabama at Birmingham, Birmingham, AL, USA

[2]Division of Human Gene Therapy, Departments of Medicine, Obstetrics and Gynecology, Pathology and Surgery, The University of Alabama at Birmingham, Birmingham, AL, USA

[3]Division of Preventive Medicine, Department of Medicine, The University of Alabama at Birmingham, Birmingham, AL, USA

[4]The Center for Metabolic Bone Disease Core Laboratory, The University of Alabama at Birmingham, Birmingham, AL, USA

[5]The Gene Therapy Center, The University of Alabama at Birmingham, Birmingham, AL, USA

Abstract

Metastatic involvement of the skeleton is a frequent consequence of advanced prostate cancer. These skeletal metastases cause a number of debilitating complications and are refractory to current treatments. New therapeutic options are being explored, including conditionally replicating adenoviruses (CRAds). CRAds are engineered to selectively replicate in and destroy tumor cells and can be “armed” with exogenous transgenes for enhanced potency. We hypothesized that a CRAd armed with osteoprotegerin (OPG), an inhibitor of osteoclastogenesis, would inhibit the progression of prostate cancer bone metastases by directly lysing tumor cells and by reducing osteoclast activity. Although prostate cancer bone metastases are predominantly osteoblastic in nature, increased osteoclast activity is critical for the growth of these lesions. Ad5-Δ24-sOPG-Fc-RGD is a CRAd that carries a fusion of the ligand-binding domains of OPG and the Fc region of human IgG1 in place of the viral E3B genes. To circumvent low tumor cell expression of the native adenoviral receptor, an arginine-glycine-aspartic acid (RGD) peptide insertion within the

Correspondence: Gene P. Siegal, M.D., Ph.D., Department of Pathology, Division of Anatomic Pathology, 508 20th Street South, HSB 149K, Birmingham, AL 35294, Phone: 205-934-6608, Fax: 205-975-7284, gsiegal@uab.edu.

*These authors contributed equally to this work.

#Present address: Department of Pediatrics, Division of Hematology and Oncology and The Gene Therapy Center, Emory University, Atlanta, GA, USA.

†Present address: Medical Scientist Training Program, Duke University, Durham, NC, USA.

‡Present address: Statistics and Epidemiology Division, Social Statistical and Environmental Sciences, RTI International, Atlanta, GA, USA.

DISCLOSURE/DUALITY OF INTEREST

The authors declare that equity in VectorLogics is held by J.T. Douglas.

viral fiber knob allows infection of cells expressing α_v integrins. A 24-base pair deletion (Δ24) within viral E1A limits replication to cells with aberrant retinoblastoma cell cycle regulator/tumor suppressor expression. We have confirmed that Ad5-Δ24-sOPG-Fc-RGD replicates within and destroys prostate cancer cells and, in both murine and human coculture models, that infection of prostate cancer cells inhibits osteoclastogenesis *in vitro*. In a murine model, progression of advanced prostate cancer bone metastases was inhibited by treatment with Ad5-Δ24-sOPG-Fc-RGD but not by an unarmed control CRAd.

Keywords

Adenovirus; bone metastasis; oncolytic virus; osteoprotegerin; prostate cancer; virotherapy

Advanced prostate cancer exhibits a propensity for metastasis to the skeleton, and thus a majority of patients with late-stage disease will be diagnosed with bone metastases (1, 2). The growth of metastatic cells in bone disrupts normal bone physiology and structure (3) and causes a range of serious complications, including pain, pathological fractures and spinal cord compression (2, 4). Current treatments with surgery, radiotherapy, chemotherapy and bisphosphonate administration may slow disease progression, but are associated with deleterious side effects (5) and are often not curative. In light of the above, new therapies for this disease are urgently needed.

One new class of anticancer agents is comprised of conditionally replicating adenoviruses (CRAds) based upon human serotype 5 (6). These are adenoviruses that have been engineered to selectively replicate within cancer cells, thereby amplifying the input dose of virus and destroying the infected tumor cells by lysis. Through multiple rounds of selective infection, replication, lysis and spread, CRAds have the potential to destroy tumors while sparing normal tissue. However, clinical trials have shown that while CRAds are safe to administer (7), their potency must be improved before the full potential of this treatment modality can be realized.

One strategy to increase the efficacy of a CRAd is to employ it as a platform for the delivery of a therapeutic transgene. Due to viral replication, an “armed” CRAd amplifies the input dose of the transgene and can exert an antitumor effect by multiple mechanisms of action. A variety of armed CRAds directed against a range of malignancies has been described, and it is clear that the inclusion of a rationally-selected transgene enhances the potency of a CRAd (8). An armed CRAd intended for prostate cancer bone metastasis will therefore be most effective when it has been selected in consideration of tumor-bone interactions. Prostate cancer bone metastases involve a disruption of normal bone homeostasis and influence the bone microenvironment in ways that are not fully understood. Prostate cancer cells produce a variety of factors including bone morphogenetic proteins, endothelin 1, and insulin-like growth factors that induce the growth of lesions which are predominantly osteoblastic in their behavior (9). However, both blastic and lytic processes are involved, and thus osteoclasts also contribute to lesion growth (10). Prostate cancer cells can mediate osteoclast formation both directly and indirectly (11), largely through the interaction of receptor activator of NF-κB ligand (RANKL) on osteoblasts with its receptor RANK on osteoclast

precursors. It has been shown that blockade of the RANK/RANKL interaction inhibits the progression of prostate cancer bone metastases (12), even those which are osteoblastic in nature (13, 14). This interaction can be disrupted by the normal bone protein osteoprotegerin (OPG), which is a soluble decoy receptor for RANKL (15, 16). OPG is secreted by osteoblasts and bone stromal cells as a key mediator of normal bone homeostasis; it prevents the binding of RANKL with RANK to inhibit osteoclast differentiation/activation and promote bone formation. Several studies have demonstrated that OPG inhibits the progression of prostate cancer bone metastases (13, 17–21). We therefore hypothesized that a CRAd armed with OPG would reduce the growth of prostate cancer bone metastases by two means: direct lysis of tumor cells due to viral replication, and a reduction in tumor burden by the inhibition of osteoclastic bone resorption by OPG.

We have previously constructed and described the armed CRAd used in this study, designated Ad5-Δ24-sOPG-Fc-RGD (22). Cancer-selective replication is conferred by means of a 24 base pair deletion in the E1A gene (23) which yields a protein unable to bind and inactivate the retinoblastoma tumor suppressor/cell cycle regulatory protein and restricts efficient viral replication to neoplastic cells. To enhance tumor cell transduction, this armed CRAd also includes a fiber knob with an RGD peptide insertion in the HI loop (24). This modification directs initial binding of the virus to $\alpha_v\beta_3$ and $\alpha_v\beta_5$ integrins, which are involved in prostate cancer bone metastasis (25, 26), and thus overcomes the deficiency of the native coxsackievirus and adenovirus receptor (CAR) on prostate cancer cells (27). This armed CRAd carries a transgene encoding the RANKL-binding domains of OPG fused to the Fc portion of human IgG1. It therefore lacks the domains of OPG that bind tumor necrosis factor-related apoptosis-inducing ligand (28), precluding its ability to act as a survival factor for prostate cancer cells (29). We have previously shown that the expression of OPG-Fc does not alter the selectivity of replication of the parent CRAd in experiments involving normal human epithelial cells and human liver slices (22).

MATERIALS AND METHODS

Cells

The human prostate cancer cell lines LNCaP (30, 31) and PC-3 (32) were purchased from the American Type Culture Collection (ATCC; Manassas, VA). The human prostate cancer cell line C4-2B, a subline of LNCaP with enhanced propensity for bone metastasis, was a gift from Dr. Leland Chung. ST2 murine bone marrow stromal cells (33) were from the Riken Cell Bank, Japan. ST2 cells were propagated in α-minimum essential medium (α-MEM) and both the LNCaP and PC3 prostate cancer cells were cultured in Roswell Park Memorial Institute (RPMI) 1640 medium. C4-2B cells were cultured in T-Medium (Invitrogen, Carlsbad, CA). These media were supplemented with 10% (v/v) heat-inactivated fetal bovine serum (FBS; Invitrogen), L-glutamine (2 mM), penicillin (100 U/ml) and streptomycin (100μg/ml). All cell lines were cultured at 37 °C in a humidified atmosphere, with ST2 cells maintained at 8% CO_2 and all others at 5% CO_2. Except where otherwise noted, media and supplements were from Mediatech (Herndon, VA).

A C4-2B cell subline which stably expresses luciferase (C4-2B-LUC) was generated by transduction of the cells with a lentiviral vector encoding the firefly luciferase gene, as

follows. 293GPG cells were cultured in Dulbecco's Modified Eagle Medium supplemented with 10% (v/v) heat-inactivated FBS, tetracycline, puromycin, G418, and penicillin/streptomycin as described previously (34). These cells were maintained exclusively in the laboratory of Xu Feng, Ph.D., in accordance with a materials transfer agreement. A plasmid, pMX-puro-Luc, was prepared by the insertion of firefly luciferase cDNA into the *Bam*HI and *Not*I restriction sites of the pMX-puro retroviral vector. Then, 293GPG cells were transiently transfected with this vector using Lipofectamine Plus reagent (Invitrogen). Virus supernatants were collected at 48, 72, and 96 h after transfection and then pooled. C4-2B cells were then infected with the viral supernatant for 24 h in the presence 8 μg/mL Polybrene (hexadimethrine bromide). The infection medium was then replaced with cell culture medium and cells were allowed to recover for 24 hours before selection with 2 μg/mL puromycin.

Viruses

The wild-type human adenovirus serotype 5, Adwt300, was purchased from ATCC. The tropism-modified control virus Ad5-RGD has wild-type E1 and E3 regions as well as an RGD peptide in the HI loop of the fiber knob and was previously generated in our laboratory (22). The two unarmed control CRAds used in this study, Ad5-Δ24 and Ad5-Δ24RGD, each have a 24 base pair deletion in the CR2 region of E1A and have been described previously (35). The tropism-modified control CRAd, Ad5-Δ24RGD, also has an RGD peptide in the HI loop of the fiber knob. The two armed CRAds used in this study, Ad5-Δ24-sOPG-Fc and Ad5-Δ24-sOPG-Fc-RGD, each carry a transgene encoding the extracellular domain of human osteoprotegerin (amino acids 1–201 (15)) fused to the Fc portion of human IgG1 (28). The transgene is in place of the E3B region of the genome, under native expression control elements. The construction of these CRAds, as well as that of the E1-deleted replication-deficient control vectors Ad-CMV-sOPG-Fc-RGD and Ad-CMV-OPG-Fc-RGD, which expresses full-length OPG, has been detailed previously (22).

Expression of sOPG and viral genes

Monolayers of C4-2B cells in 24-well plates were infected with Ad5-Δ24-sOPG-Fc, Ad5-Δ24-sOPG-Fc-RGD or Adwt300 at a multiplicity of infection (MOI) of 0.1 infectious units (IU) per cell in RPMI 1640 with 2% (v/v) FBS. Cells were incubated for 1 h at 37 °C before the infection mixtures were removed and replaced with serum-free growth medium with supplements. At various intervals post-infection (4, 8, 12, 24 and 36 h), medium was collected, and cell lysates were harvested by the addition of buffer RLT (RNeasy Mini Kit; Qiagen, Valencia, CA) to the wells. Samples were stored at −80 °C until they could be further processed.

Total cellular RNA was isolated from lysate samples using an RNeasy Mini Kit (Qiagen), according to the manufacturer's instructions. Purified RNA samples were then subjected to real-time quantitative reverse transcriptase PCR analysis using a LightCycler 480 system (Roche Diagnostics, Indianapolis, IN). Samples from cells infected with the armed CRAds were assayed for the expression of sOPG-Fc, whereas samples from cells infected with Adwt300 were assayed for expression of the E3B genes 14.7k and RIDβ (primer sequences previously published) (22). All samples were analyzed for expression of E3 gp 19k,

adenovirus death protein (ADP) and fiber. Expression of human glyceraldehyde-3-phosphate dehydrogenase was used as a control. Results are expressed as copy number/ng of total RNA.

Secretion of sOPG-Fc

Monolayers of LNCaP and C4-2B cells in 24-well plates were infected with Ad5-Δ24-sOPG-Fc or Ad5-Δ24-sOPG-Fc-RGD as above, before the infection mixtures were removed and replaced with serum-free growth medium with supplements. Medium samples were collected at various intervals post-infection (24, 36, 48 and 60 h) and stored at −80 °C. After the final time point, samples were thawed and concentrated to 1/10 of the original volume using a Microcon centrifugal filter device (Millipore, Bedford, MA) and centrifugation at 14,000 × g. The presence of sOPG-Fc was determined by SDS-PAGE followed by immunoblotting using a goat anti-human OPG primary antibody (Sigma-Aldrich, St. Louis, MO) diluted 1:1000 and a rabbit anti-goat alkaline phosphatase-conjugated secondary antibody (Jackson ImmunoResearch, West Grove, PA), diluted 1:4000. Blots were developed with 5-bromo-4-chloro-3-indolyl phosphate/nitro blue tetrazolium (BCIP/NBT; Sigma-Aldrich).

Viral DNA replication in cell lines

Monolayers of C4-2B cells in 24-well plates were infected with Adwt300, Ad5-Δ24, Ad5-Δ24RGD, Ad5-Δ24-sOPG-Fc or Ad5-Δ24-sOPG-Fc-RGD at an MOI of 0.1 IU per cell. At 2, 4 and 6 days post-infection, 200μl samples of medium were harvested and stored at −20°C until further processing. DNA was then purified from the medium samples using a QIAamp DNA Blood Mini Kit (Qiagen). Samples were analyzed by quantitative real-time PCR on a LightCycler 480 system (Roche Diagnostics) for the presence of the Ad5 E4 gene (primer sequences previously published (22)), as an indicator of viral replication (36). Results are expressed as copy number/ng of total DNA.

Cytopathic effect

In order to assay oncolytic potency qualitatively, monolayers of C4-2B, LNCaP and PC3 cells in 24-well plates were infected with Ad5-Δ24-sOPG-Fc-RGD and each of the replicating control viruses at MOIs of 1, 0.1 and 0.01 IU per cell. After 8 days, the viability of the cells was determined by staining the monolayers with 1% (w/v) crystal violet (Fisher Scientific) in 70% (v/v) ethanol for 1 h. Plates were washed in tap water to remove excess dye.

Osteoclast formation

The ability of the armed CRAds to inhibit osteoclast formation was assayed in both murine and human cells, using *in vitro* osteoclastogenesis assays that are detailed elsewhere and summarized here (22, 33). In the murine system, bone marrow macrophages were isolated from 4- to 8-week-old female athymic nude Foxn1^{nu} mice (Harlan, Indianapolis, IN) and cocultured in a 10:1 ratio with ST2 murine bone marrow stromal cells in α-MEM containing 10% (v/v) FBS, 1×10^{-8} M 1,25-dihydroxyvitamin D3 (Biomol Research Laboratories Inc., Plymouth Meeting, PA) and 1×10^{-6} M dexamethasone (Sigma-Aldrich). After a 24 h

recovery phase, porous (0.4 μm pore size) Transwell® inserts 12 mm in diameter (Corning; Corning, NY) containing monolayers of C4-2B cells that had been infected immediately prior to transfer at an MOI of 0.1 IU per cell with each of the CRAds or Ad-CMV-OPG-Fc-RGD, diluted in RPMI 1640 with 2% (v/v) FBS for 1 h, were added to these cocultures. Cultures were maintained in α-MEM supplemented with 10% (v/v) FBS, 1×10^{-8} M 1,25-dihydroxyvitamin D3 and 1×10^{-6} M dexamethasone.

In the human system, bone marrow macrophages were isolated from fresh human bone marrow purchased from Lonza (Lonza Walkersville, Walkersville, MD) and prepared as previously described (37). These cells were plated in 24 well plates and cultured in α-MEM containing 10 % FBS (v/v) supplemented with 10 ng/ml macrophage colony-stimulating factor and 25 ng/ml recombinant human RANKL (R & D Systems, Inc.) for 48 h to allow attachment. Then, monolayers of C4-2B cells cultured on porous (0.02μm pore size) 10 mm diameter Anopore® inserts (Nalge Nunc International; Rochester, NY), which had been infected immediately prior to transfer with each of the CRAds or Ad-CMV-sOPG-Fc-RGD, as above, were transferred to the 24-well plates. The cultures were maintained in α-MEM containing 10 % FBS (v/v) supplemented with macrophage colony-stimulating factor and RANKL.

The cocultures were maintained in their respective osteoclastogenic media, with conditioned medium being harvested from each well and replaced with 1 ml fresh medium every 3 days. At the completion of each experiment, the inserts carrying prostate cancer cells were stained with crystal violet. Samples of conditioned medium from day 9 were assayed for the presence of the osteoclast-specific protein tartrate-resistant acid phosphatase 5b (38) (TRAP5b) as an indicator of osteoclast formation, using a MouseTRAP or BoneTRAP ELISA kit (Immuno-diagnostic Systems Inc., Fountain Hills, AZ) for murine and human osteoclasts, respectively.

Murine model of prostate cancer bone metastasis

Animal experiments were performed in accordance with federal and institutional guidelines for animal care. Osteoblastic lesions were established by the injection of 5×10^5 C4-2B-LUC cells into the left tibiae of 4- to 5-week-old male Fox Chase SCID® beige mice (Harlan) (39). Cells were prepared for injection by detachment with Versene™followed by two washes in phosphate buffered saline (PBS) and a final resuspension in PBS at 2.5×10^7 cells/ml. Aliquots of 20 μl (5×10^5 cells) of single cell suspension were loaded into BD Micro-Fine™ IV needle (28 G) insulin syringes (3/10 cc; BD Consumer Healthcare, Franklin Lakes, NJ), which were kept on ice until the animals were ready for injection. Forty-five mice were anesthetized with 2% (v/v) isoflurane (MWI, Meridian, ID) gas at a flow rate of 0.5–1 L/min per mouse and were injected with cells in the proximal end of the left tibia. After 33 weeks, the mice were randomly divided into 3 treatment groups. Mice from two treatment groups were given intratibial injections of 2×10^6 IU of either Ad5-Δ24-sOPG-Fc-RGD ($n = 7$) or Ad5-Δ24RGD ($n = 7$) in a total volume of 20 μl of PBS. The third group of animals was injected with PBS only ($n = 6$). Three weeks after treatment, the mice were sacrificed, as were three additional age-matched control naïve mice. The left tibia of each was dissected and preserved in 10% (w/v) neutral buffered formalin (Fisher Scientific).

Tomography

For the determination of the 3-D architecture of the trabecular bone, mouse tibiae were analyzed by micro computed tomography (μCT), using a Scanco μCT40 desktop cone-beam scanner (Scanco Medical AG, Brüttisellen, Switzerland). Tibiae were placed vertically in 12 mm diameter scanning holders. Scans were performed at the following settings: 6 μm resolution, 70 kVp, 114 μA with an integration time of 200 ms. Scans were automatically reconstructed into 2-D slices, and the region of interest was outlined in each slice using the μCT Evaluation Program (v5.0A, Scanco Medical).

The scan of the trabecular bone was performed below the growth plate, and each scan consisted of 209 slices of which 100 were used for analysis. A region of interest was drawn on each of the 100 slices just inside the cortical bone, to include only the trabecular bone and marrow. Trabecular bone was thresholded at 247, to distinguish it from the marrow. The 3-D reconstruction was performed on the region of interest which only contained trabecular bone; no cortical bone was present in these regions of interest. Data was obtained on total volume (TV) of the scanned area, the volume of trabecular bone (BV) within that area, BV/TV, trabecular bone density, trabecular number, separation and thickness.

Statistical analysis

Student-Fisher *t* tests were used to analyze data from *in vitro* osteoclast formation assays. For the tomography data, a Kruskal Wallis test was used as a non-parametric alternative to ANOVA, to examine overall differences between the four groups. Since all outcomes were marginally or highly significant overall, pair wise comparisons between groups were done via Wilcoxon Two-Sample tests, to identify outcomes that were significantly different between treatments. There was no adjustment for multiple testing since these are hypothesis generating experiments. In all analyses, differences were considered significant when $P \leq 0.05$.

RESULTS

Characterization of a tropism-modified, sOPG-Fc-armed CRAd in prostate cancer cells

The genomes of the viruses used in this study are depicted in Figure 1. Ad5-Δ24-sOPG-Fc-RGD is a tropism-modified CRAd that expresses an sOPG-Fc fusion gene from the E3B region of the adenovirus genome. The sOPG-Fc transgene replaces the native E3B genes (RIDα, RIDβ and 14.7k) and was placed under native gene expression control elements. This CRAd retains expression of the E3-11.6k adenovirus death protein (ADP) for efficient lysis of infected cells and includes an RGD-modified fiber knob for enhanced transduction of tumor cells, as well as a Δ24-modified E1A gene for cancer-selective replication. An sOPG-Fc-armed CRAd with native tropism, Ad5-Δ24-sOPG-Fc, was included as a control for infectivity. Other control viruses include Ad5-Δ24 and Ad5-Δ24-RGD, unarmed CRAds with native and modified tropism, respectively. Ad5-RGD is a tropism-modified control virus that is otherwise syngeneic with the wild-type adenovirus Adwt300.

In a previous study, we demonstrated in breast cancer cells that the expression of sOPG-Fc from a CRAd mimicked that of the replaced native E3B genes, in both timing and amount

(22). Hence, we first wished to confirm these findings in prostate cancer cells. We selected for analysis the C4-2B cell line, which is a subline of LNCaP with an enhanced propensity for bone metastasis *in vivo*. C4-2B cells were infected with Ad5-Δ24-sOPG-Fc, Ad5-Δ24-sOPG-Fc-RGD or Adwt300 and cell lysates were analyzed by quantitative reverse transcriptase PCR at multiple time points post infection. The sOPG-Fc transgene was expressed late in the infection cycle, at levels similar to that of the 14.7k gene from Ad300wt (Figure 2a). Also, the expression of ADP from Ad5-Δ24-sOPG-Fc and Ad5-Δ24-sOPG-Fc-RGD is similar to that from Adwt300 in both timing and amount (Figure 2b). Together, these data indicate that the sOPG-Fc transgene is efficiently expressed in prostate cancer cells in a manner consistent with its placement in the adenoviral genome, and that the expression of surrounding viral genes is not altered.

To confirm that prostate cancer cells infected with the armed CRAds secrete sOPG-Fc into the medium, monolayers of both LNCaP and C4-2B cells were infected with Ad5-Δ24-sOPG-Fc-RGD or with Ad5-Δ24-sOPG-Fc. At multiple time points post infection, samples of conditioned medium were subjected to immunoblotting with an OPG-specific primary antibody. In samples from infected C4-2B cells, sOPG-Fc was detected in the medium beginning at 36 h postinfection (Figure 2c). LNCaP cells released sOPG-Fc into the medium at 24 h and 36 h when infected with Ad5-Δ24-sOPG-Fc-RGD or with Ad5-Δ24-sOPG-Fc, respectively (Figure 2d). In both cell lines, sOPG-Fc protein increased in amount until 60 h postinfection. These results confirm that prostate cancer cells infected with the armed CRAds efficiently secrete sOPG-Fc.

Expression of sOPG-Fc does not enhance the oncolytic potency of a CRAd in prostate cancer cells

We next sought to confirm that prostate cancer cells would support the replication of a CRAd armed with sOPG-Fc. Monolayers of C4-2B cells were infected with both the tropism-modified and -unmodified armed CRAds, their respective unarmed control CRAds, or with wild-type adenovirus. Conditioned medium was harvested 2, 4 and 6 days post infection, and DNA isolated from the samples was analyzed by quantitative real time PCR for the adenovirus E4 gene, as an indicator of viral replication. Both of the sOPG-Fc-armed CRAds replicated efficiently in the C4-2B cells, at levels similar to the unarmed CRAds and Adwt300 (Figure 3a). Thus, it is evident that the expression of sOPG-Fc from a CRAd does not enhance adenoviral replication in prostate cancer cells. To determine whether the expression of sOPG-Fc inhibits the ability of a CRAd to efficiently lyse infected prostate cancer cells, a panel of prostate cancer cells was infected with Ad5-Δ24-sOPG-Fc-RGD or control viruses. This panel included lines with low levels of CAR expression (C4-2B (40) and PC3 (41)) as well as a line expressing high levels of CAR (LNCaP (42)). After 8 days the monolayers were stained with crystal violet, in a qualitative assay for oncolytic potency. As indicated by the cleared wells resulting from viral oncolysis, all viruses were sufficiently potent to completely destroy the monolayers of each cell line at an MOI of 0.1 (Figure 3b). While most viruses completely destroyed the monolayers at the lower MOI of 0.01, the tropism-modified armed CRAd exhibited reduced oncolytic potency in comparison to its unarmed control. This result indicates that the expression of OPG does not enhance the potency of an armed CRAd in prostate cancer cells *in vitro*. This is not unexpected, since

our hypothesis predicts that the additional antitumor effect of OPG expression would be manifested only in the bone microenvironment. Considered together with the viral replication data, these experiments demonstrate that the expression of sOPG-Fc from a CRAd does not enhance viral replication or oncolytic potency in prostate cancer cells.

CRAds armed with sOPG-Fc inhibit osteoclast formation *in vitro*

Both murine and human cell culture systems were used to determine whether prostate cancer cells infected with the armed CRAds would inhibit osteoclast formation while simultaneously being lysed by viral replication. Monolayers of C4-2B cells were established on permeable cell culture inserts and then infected with the unarmed control CRAds, Ad5-Δ24 and Ad5-Δ24RGD, and both of the armed CRAds, Ad5-Δ24-sOPG-Fc or Ad5-Δ24-sOPG-Fc-RGD. Additional wells infected with tropism-modified, E1-deleted replication-deficient control vectors expressing OPG-Fc (murine experiment) or sOPG-Fc (human experiment) from the CMV promoter were included as controls for viral replication. The cell culture inserts containing the infected cells were then added either to cocultures of murine bone marrow macrophages and ST2 bone marrow stromal cells, or to cultures of human bone marrow macrophages in recombinant soluble RANKL-containing medium. In both experiments, cultures were maintained in osteoclastogenic medium and thus were expected to form osteoclasts within 7–10 days. On day 9, conditioned medium samples were analyzed by an ELISA for the osteoclast-specific protein TRAP 5b as an indicator of osteoclast formation. In both the murine (Figure 4a) and the human (Figure 4b) experiments, wells containing armed CRAds with either tropism-modified or wild-type fibers inhibited the formation of osteoclasts relative to their respective unarmed control CRAd platforms ($P < 0.05$ for all pairwise comparisons) or to the replication-defective vectors. In addition, Ad5-Δ24-sOPG-Fc-RGD inhibited the formation of osteoclasts to a greater extent than did Ad5-Δ24-sOPG-Fc in the murine cell coculture ($P < 0.05$). The monolayers containing the C4-2B cells were stained with crystal violet in order to assay cell viability. As shown for the murine experiment in Figure 4c, the cells were destroyed by the CRAds, indicating that tumor cell lysis occurs simultaneously with suppression of osteoclast formation. Overall, these findings support our hypothesis that an sOPG-Fc-armed CRAd can inhibit the growth of prostate cancer bone metastases by directly lysing tumor cells and by blocking the formation of osteoclasts.

A tropism-modified CRAd armed with sOPG-Fc inhibits prostate cancer bone metastasis *in vivo*

We next wished to demonstrate that the tropism-modified, armed CRAd, Ad5-Δ24-sOPG-Fc-RGD, could inhibit the growth of prostate cancer bone metastases *in vivo* more effectively than its unarmed control CRAd, Ad5-Δ24RGD. Osteoblastic bone metastases were established in male SCID beige mice by the injection of C4-2B-LUC cells into the left tibiae. Subsequently, a subset of mice developed rapidly-growing tumors that impaired locomotion and were removed from the study in accordance with institutional regulations. The remaining mice developed slow-growing tumors, which became palpable at approximately 9 weeks and continued to increase in size over the duration of the study. In this experiment, tumor size did not correlate with bioluminescence quantification and thus the imaging was not continued. After 33 weeks, the mice were randomly divided into three

cohorts and treated by the intratibial delivery of Ad5-Δ24RGD or Ad5-Δ24-sOPG-Fc-RGD, or given PBS only as a control. Three weeks following treatment, the mice were sacrificed and the tibiae were harvested and analyzed by μCT. The tibiae of three additional age-matched naïve mice were also harvested and examined as examples of normal bone. The average ratio of trabecular bone volume to the total analyzed volume (BV/TV), surface area of trabecular bone, and the density of the trabecular bone for each treatment group were then determined from the μCT data.

Mice in the PBS and Ad5-Δ24RGD treatment groups exhibited a loss of trabecular bone, whereas mice treated with Ad5-Δ24-sOPG-Fc-RGD displayed a trabecular structure which more closely resembled that of the naïve control mice. Images of representative tibiae from each treatment group are shown in Figure 5. Comparison of group averages revealed a number of trends. Whereas naïve mice had a BV/TV ratio of 0.0644, mice treated with PBS had ratio of 0.0223 and those treated with Ad5-Δ24-RGD had a ratio of 0.0246, representing decreases of 65% and 62%, respectively (Figure 6a). In contrast, the BV/TV ratio of Ad5-Δ24-sOPG-Fc-RGD treated mice (0.0496) was double that of the PBS and Ad5-Δ24-RGD groups, and had decreased only 23% versus the naïve group. Similarly, as shown in Figure 6b, mice treated with the armed CRAd displayed a trabecular bone surface area which more closely resembled the naïve mice (2.6982 versus 3.1104 mm^2) than did that of the PBS- (1.5437 mm^2) or Ad5-Δ24-RGD-treated mice (1.37 mm^2). Although the observed trends did not reach statistical significance by Wilcoxon Two-Sample analysis, similar findings were also observed in the examination of trabecular bone density (not shown).

In aggregate, these data show that a CRAd armed with sOPG-Fc inhibits the progression of prostate cancer bone metastases and preserves normal bone architecture more effectively than does an unarmed control CRAd, but further titration of experimental conditions will need to be performed to maximize clinical efficacy.

DISCUSSION

We have designed an armed CRAd for bone metastases that targets both the metastatic tumor cell and the bone microenvironment. Prostate cancer commonly metastasizes to the skeleton (1, 2) where it relies on increased osteoclast activity (10, 11). Thus, we hypothesized that an sOPG-Fc-armed CRAd would be effective against this disease. Here, we have confirmed that sOPG-Fc is expressed and secreted from prostate cancer cells infected with Ad5-Δ24-sOPG-Fc-RGD, and that viral replication and tumor cell lysis are not enhanced by this expression. We showed that Ad5-Δ24-sOPG-Fc-RGD inhibits osteoclastogenesis while simultaneously lysing prostate cancer cells. Finally, we have shown that Ad5-Δ24-sOPG-Fc-RGD more effectively controls the growth of established bone lesions *in vivo* than does Ad5-Δ24RGD, by more effectively preserving the normal bone architecture. Altogether, these results supported our hypothesis that a CRAd armed with OPG can inhibit the growth of prostate cancer bone metastases by directly lysing tumor cells and by reducing osteoclast formation and activation.

We focused most of our studies on the C4-2B cell line, which is a bone metastatic derivative of the LNCaP line and establishes osteoblastic lesions *in vivo* (43, 44). We also included for

analysis LNCaP cells, which were derived from a lymph node metastasis, and PC3 cells, which were isolated from a bone metastasis. We observed similar levels of gene expression, viral replication and oncolytic potency between the tropism-modified and wild-type tropism CRAds in these cell lines. The fact that each of these lines expresses CAR, with C4-2B (40) and PC3 cells (41) expressing low but detectable levels and LNCaP cells expressing high levels (42) may explain these results. Although our *in vitro* experiments did not show a clear advantage in the use of the tropism-modified armed CRAd over its wild-type fiber control, a study by Rauen *et al*. showed that the expression of CAR in prostate tumors is inversely correlated with tumor stage/aggressiveness (27). Interestingly, CAR was detected in the four bone metastasis specimens analyzed but expression was not uniform. Regardless, the RGD tropism modification does not preclude binding of the virus to CAR (24). Therefore, the RGD-modified armed CRAd, with its expanded tropism, would likely be a more effective therapeutic than an isogenic CRAd with wild-type fibers. In our osteoclastogenesis experiments, cell death was observed in C4-2B cells infected with the non-replicative control vector. We speculate that this may have resulted from a toxic effect by some mechanism unrelated to replication; the reason for this cell death was not determined. Considered together with the oncolytic potency experiments, however, the data nonetheless show that an OPG-armed CRAd is capable of simultaneously destroying tumor cells by lysis while mediating an inhibition of osteoclastogenesis, consistent with our previous findings (22).

For our *in vivo* experiment, we developed a C4-2B cell line which stably expresses luciferase. Our intention was to monitor tumor growth non-invasively by bioluminescence imaging. However, tumor luciferase expression did not correlate with tumor growth, and thus we were unable to rely upon imaging for tumor monitoring. This lack of correlation may have been due to the long time frame of the experiment, which may have allowed for a loss of luciferase expression. We observed the C4-2B tumors to be slow growing *in vivo*, which has been noted by others using this line (44–48). As in other intra-osseous murine models of prostate cancer bone metastases, progression is typically observed over periods of weeks to months, particularly in studies employing the LNCaP line and its derivatives (39, 44, 49–53). At the conclusion of our experiment, we observed extensive trabecular bone destruction rather than osteosclerosis, as indicated by an overall loss of trabecular bone in all treatment groups. This effect was also reported by Chanda *et al*., in a study demonstrating that intratibial tumors of C4-2B cells converted from an osteoblastic to an osteolytic phenotype after 6 months *in vivo* (48). In a rat model of prostate cancer bone metastasis, Lynch *et al.* showed that osteoclast numbers increased in mixed lesions up to 4 weeks, when the experiment was concluded (54). This suggests that after an initial osteoblastic phase, the constant upregulation of osteoclast activity leads to an overall loss of bone in mature lesions. The biphasic growth of prostate cancer bone metastases may account for the contradictory roles of OPG in their development. Prostate cancer cell lines, including PC3, LNCaP (29) and C4-2B (55), express OPG. This expression may promote tumor cell survival and bone formation initially, but is nonetheless insufficient to prevent the eventual loss of bone in mature lesions.

We intended to treat well-established tumors and therefore administered treatment at week 33. By treating established tumors, this was a more challenging model but one that more closely represented a clinical scenario. A variety of studies have examined the potential of OPG for the treatment of bone metastases of prostate cancer in murine models. These include studies in which OPG expression within a prostate cancer bone lesion inhibited both osteoblastic (19) and osteolytic (48) tumor progression and others involving the use of recombinant OPG (17, 18, 20, 53, 56) in intratibial models of prostate bone metastases. In these models, which include the osteolytic PC3 model (14, 20) and the osteoblastic LNCaP (18) and C4-2B (17) models, it has consistently been shown that the administration of recombinant OPG to tumor-bearing mice significantly reduces the growth of established intratibial lesions, but does not inhibit the growth of prostate cancer cells *in vitro* or the growth of subcutaneous xenografts. Two reports have implicated extracellular calcium in the growth of prostate cancer bone metastases (57, 58), suggesting that the inhibition of bone resorption by factors such as OPG, by means of calcium depletion, may contribute to a reduction in prostate cancer bone metastasis. However, because OPG does not affect proliferation of prostate cancer cells, and is not directly cytotoxic, it is unlikely that OPG administration alone would be sufficient to eliminate established metastases. Regarding safety, it is possible that the expression of OPG from a CRAd could influence the surrounding normal bone, with the most likely effect being a transient increase in bone formation. However, OPG was safely given to multiple myeloma and breast cancer patients in a Phase I trial (59).

For both tumor cell implantation and delivery of the CRAds, we utilized intratibial injection (39). This method is frequently employed in models of prostate cancer bone metastasis, as systemic and orthotopic prostate cancer models do not efficiently establish bone metastases (44, 60). This delivery method may have limited the antitumor effect that we were able to achieve, as the small size of the intratibial compartment limited the amount of virus that could be injected. Intratibial injection was a practical necessity, however, because the systemic delivery of adenovirus is unfeasible from a clinical standpoint, as intravenously delivered adenoviruses are largely sequestered by the liver (61). As work continues in the field of adenoviral targeting, this problem may be overcome in the future. In the μCT analysis of the tumor-bearing tibiae, we observed a wide variability within treatment groups that prevented the observed trends from reaching statistical significance. This limitation of the intratibial tumor model has been reported by others (62). Although the observed trends were consistent across all measurements, larger treatment groups would have made statistical significance easier to attain. However, it is also likely that, due to inherently variable growth rates of tumors *in vivo*, unacceptably large numbers of mice might have been necessary, suggesting that better animal models are an additional requirement to move the field forward. Finally, this study was designed to examine certain endpoints. An expanded study in which samples are harvested at specific time points to examine dynamic changes in viral replication and tumor/bone interactions would reveal valuable information that would guide the clinical application of this CRAd.

We have demonstrated the potential utility of an sOPG-Fc-armed CRAd as a treatment for prostate cancer bone metastases. A number of studies have been published regarding the use

of oncolytic viruses for prostate cancer and have been reviewed by Fukuhara *et al*. (63). In particular, studies involving CRAds in models of prostate cancer bone metastasis (64, 65), including one employing the C4-2B model (66) and one in which CRAds armed with a soluble transforming growth factor beta receptor II-Fc fusions are used in a PC3 model (67), have underscored the potential for this treatment strategy. This report, however, is the first to evaluate an armed CRAd designed specifically for the bone microenvironment in a model of prostate cancer bone metastases. Furthermore, it is likely that this CRAd, Ad5-Δ24-sOPG-Fc-RGD, will also be effective against other malignancies that metastasize to the skeleton such as lung, thyroid, or renal carcinomas.

Acknowledgments

Sources of support: National Institutes of Health Grants R01 CA108585 and T32 CA075930

The authors would like to acknowledge Xingsheng Li, Ph.D. and Maria S. Johnson, Ph.D. at the Small Animal Bone Phenotyping Core facility in the UAB Center for Metabolic Bone Disease for technical assistance with the μCT analysis.

This work was supported by National Institutes of Health Grants R01 CA108585 and T32 CA075930

Abbreviations

ADP	adenovirus death protein
BV	bone volume
CAR	coxsackievirus and adenovirus receptor
CRAd	conditionally replicating adenovirus
μCT	micro computed tomography
FBS	fetal bovine serum
IU	infectious unit
MEM	minimum essential medium
MOI	multiplicity of infection
OPG	osteoprotegerin
PBS	phosphate buffered saline
RANK	receptor activator of nuclear factor (NF) kappa B
RANKL	RANK ligand
RPMI	Roswell Park Memorial Institute
TRAP5b	tartrate-resistant acid phosphatase 5b
TV	total volume

References

1. Bubendorf L, Schopfer A, Wagner U, Sauter G, Moch H, Willi N, Gasser TC, Mihatsch MJ. Metastatic patterns of prostate cancer: an autopsy study of 1,589 patients. Hum Pathol. 2000; 31:578–83. [PubMed: 10836297]
2. Coleman RE. Clinical features of metastatic bone disease and risk of skeletal morbidity. Clin Cancer Res. 2006; 12:6243s–9s. [PubMed: 17062708]
3. Roudier MP, Vesselle H, True LD, Higano CS, Ott SM, King SH, Vessella RL. Bone histology at autopsy and matched bone scintigraphy findings in patients with hormone refractory prostate cancer: the effect of bisphosphonate therapy on bone scintigraphy results. Clin Exp Metastasis. 2003; 20:171–80. [PubMed: 12705638]
4. Coleman RE. Metastatic bone disease: clinical features, pathophysiology and treatment strategies. Cancer Treat Rev. 2001; 27:165–76. [PubMed: 11417967]
5. James ND, Bloomfield D, Luscombe C. The changing pattern of management for hormone-refractory, metastatic prostate cancer. Prostate Cancer Prostatic Dis. 2006; 9:221–9. [PubMed: 16801939]
6. Alemany R, Balague C, Curiel DT. Replicative adenoviruses for cancer therapy. Nat Biotechnol. 2000; 18:723–7. [PubMed: 10888838]
7. Kirn D. Clinical research results with dl1520 (Onyx-015), a replication-selective adenovirus for the treatment of cancer: what have we learned? Gene Ther. 2001; 8:89–98. [PubMed: 11313778]
8. Cody JJ, Douglas JT. Armed replicating adenoviruses for cancer virotherapy. Cancer Gene Ther. 2009; 16:473–88. [PubMed: 19197323]
9. Mundy GR. Metastasis to bone: causes, consequences and therapeutic opportunities. Nat Rev Cancer. 2002; 2:584–93. [PubMed: 12154351]
10. Roato I, D'Amelio P, Gorassini E, Grimaldi A, Bonello L, Fiori C, Delsedime L, Tizzani A, De Libero A, Isaia G, Ferracini R. Osteoclasts are active in bone forming metastases of prostate cancer patients. PLoS One. 2008; 3:e3627. [PubMed: 18978943]
11. Inoue H, Nishimura K, Oka D, Nakai Y, Shiba M, Tokizane T, Arai Y, Nakayama M, Shimizu K, Takaha N, Nonomura N, Okuyama A. Prostate cancer mediates osteoclastogenesis through two different pathways. Cancer Lett. 2005; 223:121–8. [PubMed: 15890244]
12. Zhang J, Dai J, Yao Z, Lu Y, Dougall W, Keller ET. Soluble receptor activator of nuclear factor kappaB Fc diminishes prostate cancer progression in bone. Cancer Res. 2003; 63:7883–90. [PubMed: 14633717]
13. Yonou H, Kanomata N, Goya M, Kamijo T, Yokose T, Hasebe T, Nagai K, Hatano T, Ogawa Y, Ochiai A. Osteoprotegerin/osteoclastogenesis inhibitory factor decreases human prostate cancer burden in human adult bone implanted into nonobese diabetic/severe combined immunodeficient mice. Cancer Res. 2003; 63:2096–102. [PubMed: 12727825]
14. Whang PG, Schwarz EM, Gamradt SC, Dougall WC, Lieberman JR. The effects of RANK blockade and osteoclast depletion in a model of pure osteoblastic prostate cancer metastasis in bone. J Orthop Res. 2005; 23:1475–83. [PubMed: 16005175]
15. Simonet WS, Lacey DL, Dunstan CR, Kelley M, Chang MS, Luthy R, Nguyen HQ, Wooden S, Bennett L, Boone T, Shimamoto G, DeRose M, Elliott R, Colombero A, Tan HL, Trail G, Sullivan J, Davy E, Bucay N, Renshaw-Gegg L, Hughes TM, Hill D, Pattison W, Campbell P, Boyle WJ, et al. Osteoprotegerin: a novel secreted protein involved in the regulation of bone density. Cell. 1997; 89:309–19. [PubMed: 9108485]
16. Udagawa N, Takahashi N, Yasuda H, Mizuno A, Itoh K, Ueno Y, Shinki T, Gillespie MT, Martin TJ, Higashio K, Suda T. Osteoprotegerin produced by osteoblasts is an important regulator in osteoclast development and function. Endocrinology. 2000; 141:3478–84. [PubMed: 10965921]
17. Zhang J, Dai J, Qi Y, Lin DL, Smith P, Strayhorn C, Mizokami A, Fu Z, Westman J, Keller ET. Osteoprotegerin inhibits prostate cancer-induced osteoclastogenesis and prevents prostate tumor growth in the bone. J Clin Invest. 2001; 107:1235–44. [PubMed: 11375413]
18. Kiefer JA, Vessella RL, Quinn JE, Odman AM, Zhang J, Keller ET, Kostenuik PJ, Dunstan CR, Corey E. The effect of osteoprotegerin administration on the intra-tibial growth of the osteoblastic

LuCaP 23. 1 prostate cancer xenograft. Clin Exp Metastasis. 2004; 21:381–7. [PubMed: 15672862]

19. Corey E, Brown LG, Kiefer JA, Quinn JE, Pitts TE, Blair JM, Vessella RL. Osteoprotegerin in prostate cancer bone metastasis. Cancer Res. 2005; 65:1710–8. [PubMed: 15753366]
20. Armstrong AP, Miller RE, Jones JC, Zhang J, Keller ET, Dougall WC. RANKL acts directly on RANK-expressing prostate tumor cells and mediates migration and expression of tumor metastasis genes. Prostate. 2008; 68:92–104. [PubMed: 18008334]
21. Miller RE, Roudier M, Jones J, Armstrong A, Canon J, Dougall WC. RANK ligand inhibition plus docetaxel improves survival and reduces tumor burden in a murine model of prostate cancer bone metastasis. Mol Cancer Ther. 2008; 7:2160–9. [PubMed: 18606716]
22. Cody JJ, Rivera AA, Lyons GR, Yang SW, Wang M, Sarver DB, Wang D, Selander KS, Kuo HC, Meleth S, Feng X, Siegal GP, Douglas JT. Arming a replicating adenovirus with osteoprotegerin reduces the tumor burden in a murine model of osteolytic bone metastases of breast cancer. Cancer Gene Ther. 2010; 17:893–905. [PubMed: 20798695]
23. Fueyo J, Gomez-Manzano C, Alemany R, Lee PS, McDonnell TJ, Mitlianga P, Shi YX, Levin VA, Yung WK, Kyritsis AP. A mutant oncolytic adenovirus targeting the Rb pathway produces anti-glioma effect in vivo. Oncogene. 2000; 19:2–12. [PubMed: 10644974]
24. Dmitriev I, Krasnykh V, Miller CR, Wang M, Kashentseva E, Mikheeva G, Belousova N, Curiel DT. An adenovirus vector with genetically modified fibers demonstrates expanded tropism via utilization of a coxsackievirus and adenovirus receptor-independent cell entry mechanism. J Virol. 1998; 72:9706–13. [PubMed: 9811704]
25. Cooper CR, Chay CH, Pienta KJ. The role of alpha(v)beta(3) in prostate cancer progression. Neoplasia. 2002; 4:191–4. [PubMed: 11988838]
26. Bisanz K, Yu J, Edlund M, Spohn B, Hung MC, Chung LW, Hsieh CL. Targeting ECM-integrin interaction with liposome-encapsulated small interfering RNAs inhibits the growth of human prostate cancer in a bone xenograft imaging model. Mol Ther. 2005; 12:634–43. [PubMed: 16039164]
27. Rauen KA, Sudilovsky D, Le JL, Chew KL, Hann B, Weinberg V, Schmitt LD, McCormick F. Expression of the coxsackie adenovirus receptor in normal prostate and in primary and metastatic prostate carcinoma: potential relevance to gene therapy. Cancer Res. 2002; 62:3812–8. [PubMed: 12097294]
28. Emery JG, McDonnell P, Burke MB, Deen KC, Lyn S, Silverman C, Dul E, Appelbaum ER, Eichman C, DiPrinzio R, Dodds RA, James IE, Rosenberg M, Lee JC, Young PR. Osteoprotegerin is a receptor for the cytotoxic ligand TRAIL. J Biol Chem. 1998; 273:14363–7. [PubMed: 9603945]
29. Holen I, Croucher PI, Hamdy FC, Eaton CL. Osteoprotegerin (OPG) is a survival factor for human prostate cancer cells. Cancer Res. 2002; 62:1619–23. [PubMed: 11912131]
30. Horoszewicz JS, Leong SS, Chu TM, Wajsman ZL, Friedman M, Papsidero L, Kim U, Chai LS, Kakati S, Arya SK, Sandberg AA. The LNCaP cell line--a new model for studies on human prostatic carcinoma. Prog Clin Biol Res. 1980; 37:115–32. [PubMed: 7384082]
31. Horoszewicz JS, Leong SS, Kawinski E, Karr JP, Rosenthal H, Chu TM, Mirand EA, Murphy GP. LNCaP model of human prostatic carcinoma. Cancer Res. 1983; 43:1809–18. [PubMed: 6831420]
32. Kaighn ME, Narayan KS, Ohnuki Y, Lechner JF, Jones LW. Establishment and characterization of a human prostatic carcinoma cell line (PC-3). Invest Urol. 1979; 17:16–23. [PubMed: 447482]
33. Udagawa N, Takahashi N, Akatsu T, Sasaki T, Yamaguchi A, Kodama H, Martin TJ, Suda T. The bone marrow-derived stromal cell lines MC3T3-G2/PA6 and ST2 support osteoclast-like cell differentiation in cocultures with mouse spleen cells. Endocrinology. 1989; 125:1805–13. [PubMed: 2676473]
34. Ory DS, Neugeboren BA, Mulligan RC. A stable human-derived packaging cell line for production of high titer retrovirus/vesicular stomatitis virus G pseudotypes. Proc Natl Acad Sci U S A. 1996; 93:11400–6. [PubMed: 8876147]
35. Suzuki K, Alemany R, Yamamoto M, Curiel DT. The presence of the adenovirus E3 region improves the oncolytic potency of conditionally replicative adenoviruses. Clin Cancer Res. 2002; 8:3348–59. [PubMed: 12429621]

36. Rivera AA, Wang M, Suzuki K, Uil TG, Krasnykh V, Curiel DT, Nettelbeck DM. Mode of transgene expression after fusion to early or late viral genes of a conditionally replicating adenovirus via an optimized internal ribosome entry site in vitro and in vivo. Virology. 2004; 320:121–34. [PubMed: 15003868]

37. Cody JJ, Rivera AA, Liu J, Liu JM, Douglas JT, Feng X. A simplified method for the generation of human osteoclasts in vitro. Int J Biochem Mol Biol. 2011; 2:183–9. [PubMed: 21968748]

38. Halleen JM, Alatalo SL, Suominen H, Cheng S, Janckila AJ, Vaananen HK. Tartrate-resistant acid phosphatase 5b: a novel serum marker of bone resorption. J Bone Miner Res. 2000; 15:1337–45. [PubMed: 10893682]

39. Corey E, Quinn JE, Bladou F, Brown LG, Roudier MP, Brown JM, Buhler KR, Vessella RL. Establishment and characterization of osseous prostate cancer models: intra-tibial injection of human prostate cancer cells. Prostate. 2002; 52:20–33. [PubMed: 11992617]

40. Kasman L, Onicescu G, Voelkel-Johnson C. Histone deacetylase inhibitors restore cell surface expression of the coxsackie adenovirus receptor and enhance CMV promoter activity in castration-resistant prostate cancer cells. Prostate Cancer. 2012; 2012:137163. [PubMed: 22288017]

41. Pandha HS, Stockwin LH, Eaton J, Clarke IA, Dalgleish AG, Todryk SM, Blair GE. Coxsackie B and adenovirus receptor, integrin and major histocompatibility complex class I expression in human prostate cancer cell lines: implications for gene therapy strategies. Prostate Cancer Prostatic Dis. 2003; 6:6–11. [PubMed: 12664058]

42. Seki T, Dmitriev I, Suzuki K, Kashentseva E, Takayama K, Rots M, Uil T, Wu H, Wang M, Curiel DT. Fiber shaft extension in combination with HI loop ligands augments infectivity for CAR-negative tumor targets but does not enhance hepatotropism in vivo. Gene Ther. 2002; 9:1101–8. [PubMed: 12140738]

43. Thalmann GN, Anezinis PE, Chang SM, Zhau HE, Kim EE, Hopwood VL, Pathak S, von Eschenbach AC, Chung LW. Androgen-independent cancer progression and bone metastasis in the LNCaP model of human prostate cancer. Cancer Res. 1994; 54:2577–81. [PubMed: 8168083]

44. Wu TT, Sikes RA, Cui Q, Thalmann GN, Kao C, Murphy CF, Yang H, Zhau HE, Balian G, Chung LW. Establishing human prostate cancer cell xenografts in bone: induction of osteoblastic reaction by prostate-specific antigen-producing tumors in athymic and SCID/bg mice using LNCaP and lineage-derived metastatic sublines. Int J Cancer. 1998; 77:887–94. [PubMed: 9714059]

45. Hall CL, Bafico A, Dai J, Aaronson SA, Keller ET. Prostate cancer cells promote osteoblastic bone metastases through Wnts. Cancer Res. 2005; 65:7554–60. [PubMed: 16140917]

46. Kitagawa Y, Dai J, Zhang J, Keller JM, Nor J, Yao Z, Keller ET. Vascular endothelial growth factor contributes to prostate cancer-mediated osteoblastic activity. Cancer Res. 2005; 65:10921–9. [PubMed: 16322239]

47. Rubin J, Fan X, Rahnert J, Sen B, Hsieh CL, Murphy TC, Nanes MS, Horton LG, Beamer WG, Rosen CJ. IGF-I secretion by prostate carcinoma cells does not alter tumor-bone cell interactions in vitro or in vivo. Prostate. 2006; 66:789–800. [PubMed: 16482567]

48. Chanda D, Isayeva T, Kumar S, Hensel JA, Sawant A, Ramaswamy G, Siegal GP, Beatty MS, Ponnazhagan S. Therapeutic potential of adult bone marrow-derived mesenchymal stem cells in prostate cancer bone metastasis. Clin Cancer Res. 2009; 15:7175–85. [PubMed: 19920103]

49. Fizazi K, Yang J, Peleg S, Sikes CR, Kreimann EL, Daliani D, Olive M, Raymond KA, Janus TJ, Logothetis CJ, Karsenty G, Navone NM. Prostate cancer cells-osteoblast interaction shifts expression of growth/survival-related genes in prostate cancer and reduces expression of osteoprotegerin in osteoblasts. Clin Cancer Res. 2003; 9:2587–97. [PubMed: 12855635]

50. Burton DW, Geller J, Yang M, Jiang P, Barken I, Hastings RH, Hoffman RM, Deftos LJ. Monitoring of skeletal progression of prostate cancer by GFP imaging, X-ray, and serum OPG and PTHrP. Prostate. 2005; 62:275–81. [PubMed: 15389781]

51. Yang M, Burton DW, Geller J, Hillegonds DJ, Hastings RH, Deftos LJ, Hoffman RM. The bisphosphonate olpadronate inhibits skeletal prostate cancer progression in a green fluorescent protein nude mouse model. Clin Cancer Res. 2006; 12:2602–6. [PubMed: 16638872]

52. Bonfil RD, Dong Z, Trindade Filho JC, Sabbota A, Osenkowski P, Nabha S, Yamamoto H, Chinni SR, Zhao H, Mobashery S, Vessella RL, Fridman R, Cher ML. Prostate cancer-associated

membrane type 1-matrix metalloproteinase: a pivotal role in bone response and intraosseous tumor growth. Am J Pathol. 2007; 170:2100–11. [PubMed: 17525276]

53. Morrissey C, Kostenuik PL, Brown LG, Vessella RL, Corey E. Host-derived RANKL is responsible for osteolysis in a C4-2 human prostate cancer xenograft model of experimental bone metastases. BMC Cancer. 2007; 7:148. [PubMed: 17683568]
54. Lynch CC, Hikosaka A, Acuff HB, Martin MD, Kawai N, Singh RK, Vargo-Gogola TC, Begtrup JL, Peterson TE, Fingleton B, Shirai T, Matrisian LM, Futakuchi M. MMP-7 promotes prostate cancer-induced osteolysis via the solubilization of RANKL. Cancer Cell. 2005; 7:485–96. [PubMed: 15894268]
55. Lin DL, Tarnowski CP, Zhang J, Dai J, Rohn E, Patel AH, Morris MD, Keller ET. Bone metastatic LNCaP-derivative C4-2B prostate cancer cell line mineralizes in vitro. Prostate. 2001; 47:212–21. [PubMed: 11351351]
56. Quinn JE, Brown LG, Zhang J, Keller ET, Vessella RL, Corey E. Comparison of Fc-osteoprotegerin and zoledronic acid activities suggests that zoledronic acid inhibits prostate cancer in bone by indirect mechanisms. Prostate Cancer Prostatic Dis. 2005; 8:253–9. [PubMed: 15999121]
57. Li X, Liao J, Park SI, Koh AJ, Sadler WD, Pienta KJ, Rosol TJ, McCauley LK. Drugs which inhibit osteoclast function suppress tumor growth through calcium reduction in bone. Bone. 2011
58. Liao J, Schneider A, Datta NS, McCauley LK. Extracellular calcium as a candidate mediator of prostate cancer skeletal metastasis. Cancer Res. 2006; 66:9065–73. [PubMed: 16982748]
59. Body JJ, Greipp P, Coleman RE, Facon T, Geurs F, Fermand JP, Harousseau JL, Lipton A, Mariette X, Williams CD, Nakanishi A, Holloway D, Martin SW, Dunstan CR, Bekker PJ. A phase I study of AMGN-0007, a recombinant osteoprotegerin construct, in patients with multiple myeloma or breast carcinoma related bone metastases. Cancer. 2003; 97:887–92. [PubMed: 12548591]
60. Singh AS, Figg WD. In vivo models of prostate cancer metastasis to bone. J Urol. 2005; 174:820–6. [PubMed: 16093963]
61. Glasgow JN, Everts M, Curiel DT. Transductional targeting of adenovirus vectors for gene therapy. Cancer Gene Ther. 2006; 13:830–44. [PubMed: 16439993]
62. Canon JR, Roudier M, Bryant R, Morony S, Stolina M, Kostenuik PJ, Dougall WC. Inhibition of RANKL blocks skeletal tumor progression and improves survival in a mouse model of breast cancer bone metastasis. Clin Exp Metastasis. 2008; 25:119–29. [PubMed: 18064531]
63. Fukuhara H, Homma Y, Todo T. Oncolytic virus therapy for prostate cancer. Int J Urol. 2010; 17:20–30. [PubMed: 19832925]
64. Matsubara S, Wada Y, Gardner TA, Egawa M, Park MS, Hsieh CL, Zhau HE, Kao C, Kamidono S, Gillenwater JY, Chung LW. A conditional replication-competent adenoviral vector, Ad-OC-E1a, to cotarget prostate cancer and bone stroma in an experimental model of androgen-independent prostate cancer bone metastasis. Cancer Res. 2001; 61:6012–9. [PubMed: 11507044]
65. Sandberg L, Papareddy P, Silver J, Bergh A, Mei YF. Replication-competent Ad11p vector (RCAd11p) efficiently transduces and replicates in hormone-refractory metastatic prostate cancer cells. Hum Gene Ther. 2009; 20:361–73. [PubMed: 19199789]
66. Li Y, Kacka M, Thompson M, Hsieh JT, Koeneman KS. Conditionally replicating adenovirus therapy utilizing bone sialoprotein promoter (Ad-BSP-E1a) in an in vivo study of treating androgen-independent intraosseous prostate cancer. Urol Oncol. 2009
67. Seth P, Hu Z, Gupta J, Zhang Z, Gerseny H, Berg A, Chen YJ, Du H, Brendler CB, Xiao X, Pienta KJ, Guise T, Lee C, Stern PH, Stock S. Systemic Delivery of Oncolytic Adenoviruses Targeting Transforming Growth Factor Beta Inhibits Established Bone Metastasis in a Prostate Cancer Mouse Model. Hum Gene Ther. 2012

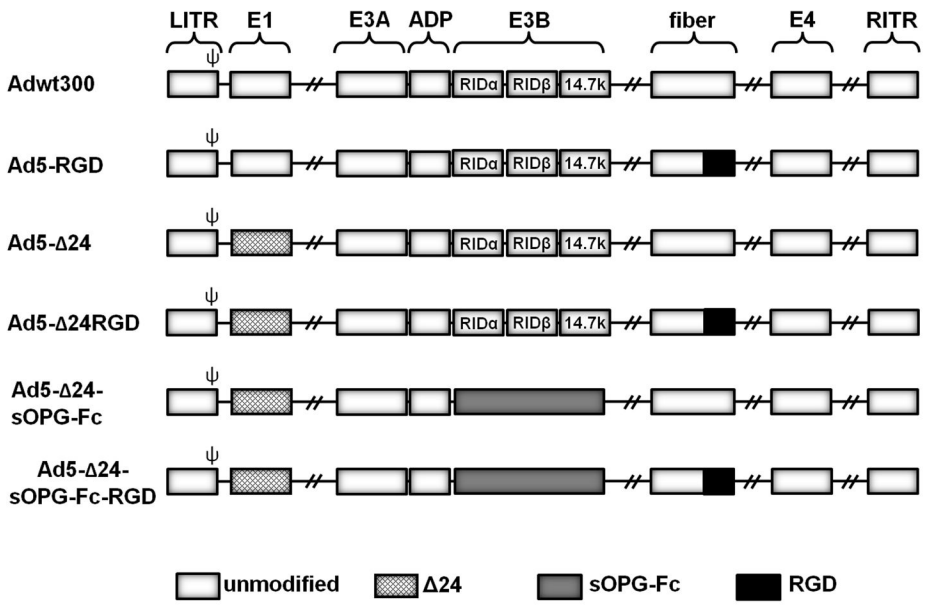

Fig. 1.

The genomes of the viruses used in this study are represented schematically. By convention, the adenovirus genome is depicted as having (from left to right): a left inverted terminal repeat (LITR) containing the packaging signal (ψ), the early 1 (E1) gene, E3A region, adenovirus death protein (ADP), E3B region (containing the receptor internalization and degradation alpha [RIDα], RIDβ and 14.7k genes), fiber gene, E4 gene, and right inverted terminal repeat (RITR). For clarity, additional adenoviral genes are not shown. Modifications made to specific viruses, as indicated, include a 24-base pair deletion within E1 (Δ24), replacement of E3B with an sOPG-Fc fusion gene, and the inclusion of a RGD peptide within the knob domain of the fiber

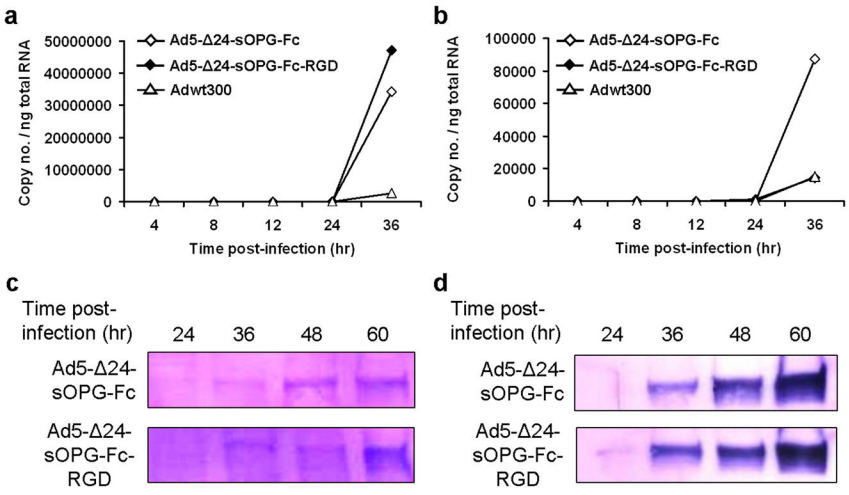

Fig. 2.

Characterization of armed CRAds. *a*, *b*, C4-2B prostate cancer cells were infected with Ad5-Δ24-sOPG-Fc, Ad5-Δ24-sOPG-Fc-RGD or Adwt300. At the indicated times post-infection, total cellular RNA was extracted and subjected to quantitative reverse transcriptase PCR to detect expression of: *a*, the sOPG-Fc gene (for cells infected with Ad5-Δ24-sOPGFc or Ad5-Δ24-sOPG-Fc-RGD) or the 14.7k gene (for cells infected with Adwt300); and *b*, the ADP gene. *c*, *d*, Secretion of sOPG-Fc by infected C4-2B (*c*) and LNCaP (*d*) cells. At the indicated times post-infection, conditioned medium was harvested and subjected to immunoblot analysis using an anti-OPG primary antibody

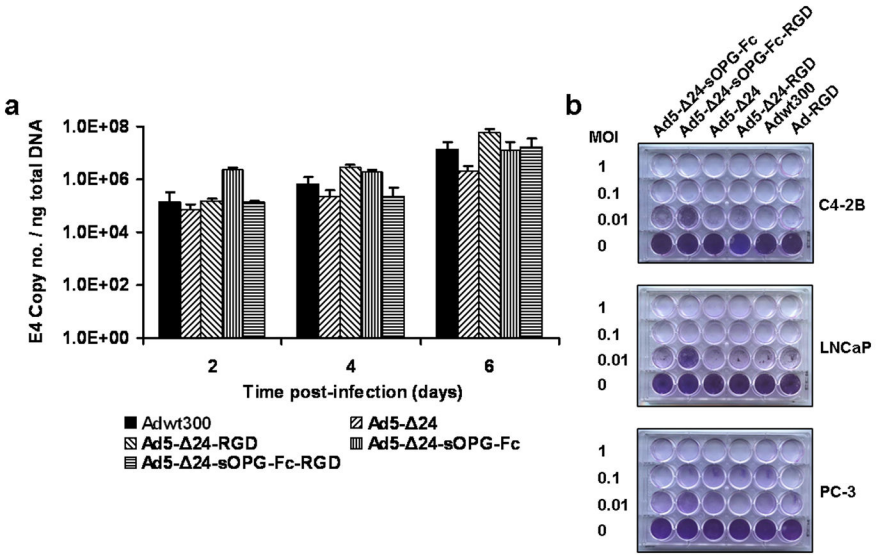

Fig. 3.

Oncolytic potency of the armed CRAds. *a*, C4-2B prostate cancer cells were infected with Adwt300, Ad5-Δ24, Ad5-Δ24RGD, Ad5-Δ24-sOPG-Fc or Ad5-Δ24-sOPG-Fc-RGD. The conditioned culture medium was harvested at 2, 4 and 6 days post-infection. DNA was extracted and subjected to Q-PCR to detect the E4 gene as a measure of viral DNA replication. Results are the means ± SD of duplicate determinations. Representative results of 3 separate experiments are shown. *b*, a panel of prostate cancer cell lines was infected at the indicated MOIs. Eight days post-infection, viable cells were fixed and stained with crystal violet. Representative results of 3 separate experiments are shown

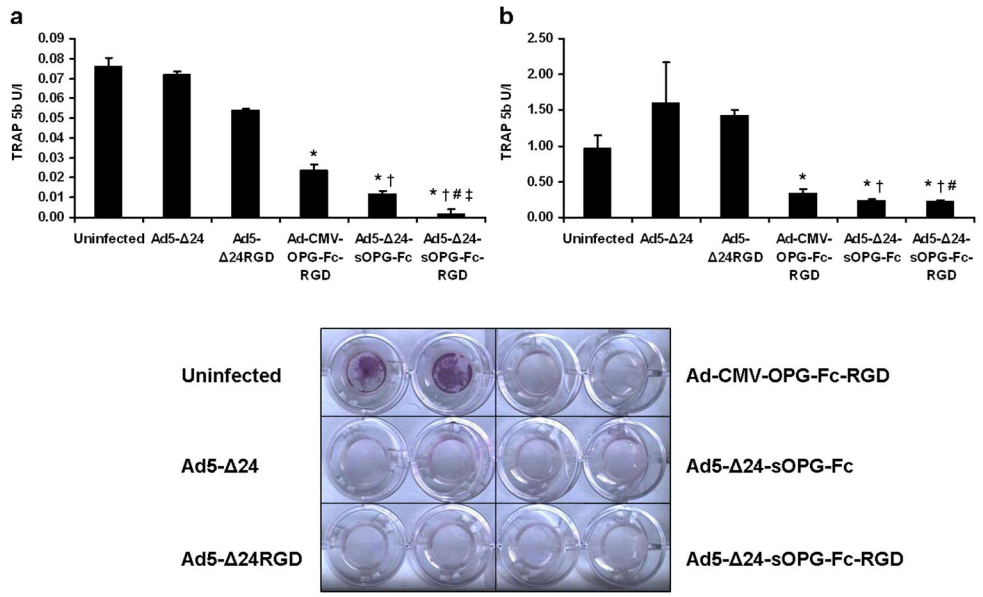

Fig. 4.

CRAds armed with sOPG-Fc simultaneously lyse prostate cancer cells and inhibit osteoclast formation *in vitro*. C4-2B cells were infected with the indicated adenoviruses and grown on inserts overlaying cocultures of murine osteoclast precursors and ST2 bone marrow stromal cells (*a*), or human osteoclast precursors and RANKL (*b*). At day 9, an ELISA was performed to detect TRAP5b, an osteoclast marker protein. Results are means ± SD of duplicate determinations. Significant differences ($P < 0.05$) versus uninfected (*), unarmed CRAd (†), non-replicative vector (#), and armed CRAd with native tropism (‡) are indicated. Representative results of 2 separate experiments are shown. *c*, Viable prostate cancer cells on the inserts were fixed and stained with crystal violet

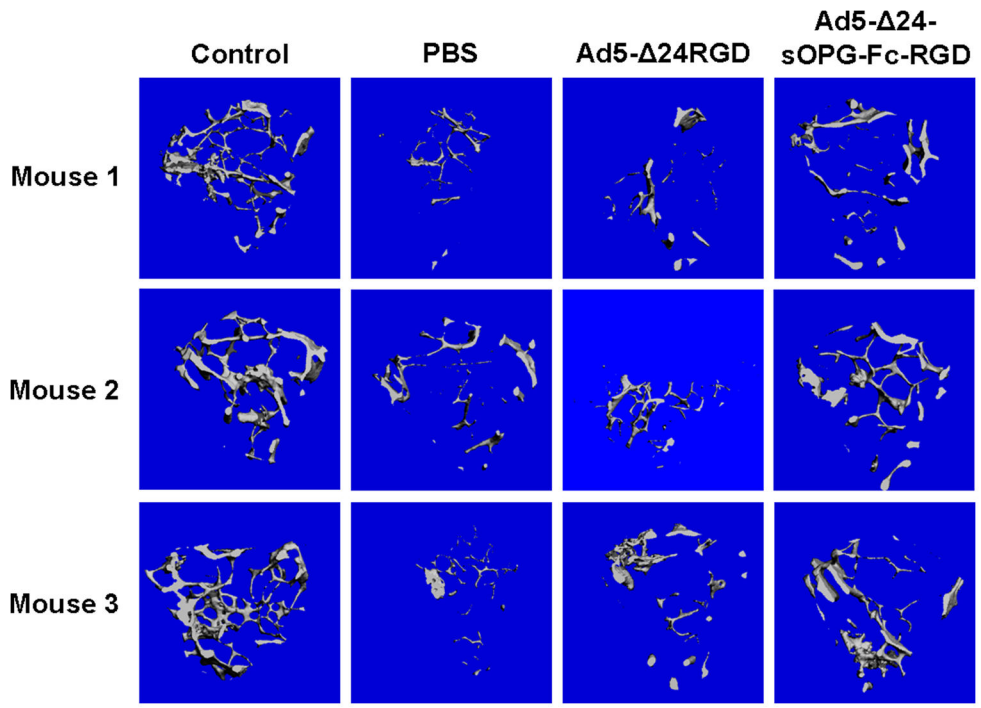

Fig. 5.

An sOPG-Fc-armed CRAd inhibits the progression of bone metastases of prostate cancer *in vivo* more effectively than does an unarmed CRAd. Intratibial tumors of C4-2B-LUC prostate cancer cells were established in SCID mice and treated with either Ad5-Δ24-sOPG-Fc-RGD, Ad5-Δ24RGD or PBS. Shown are μCT images of the proximal tibiae of three representative mice from each treatment group

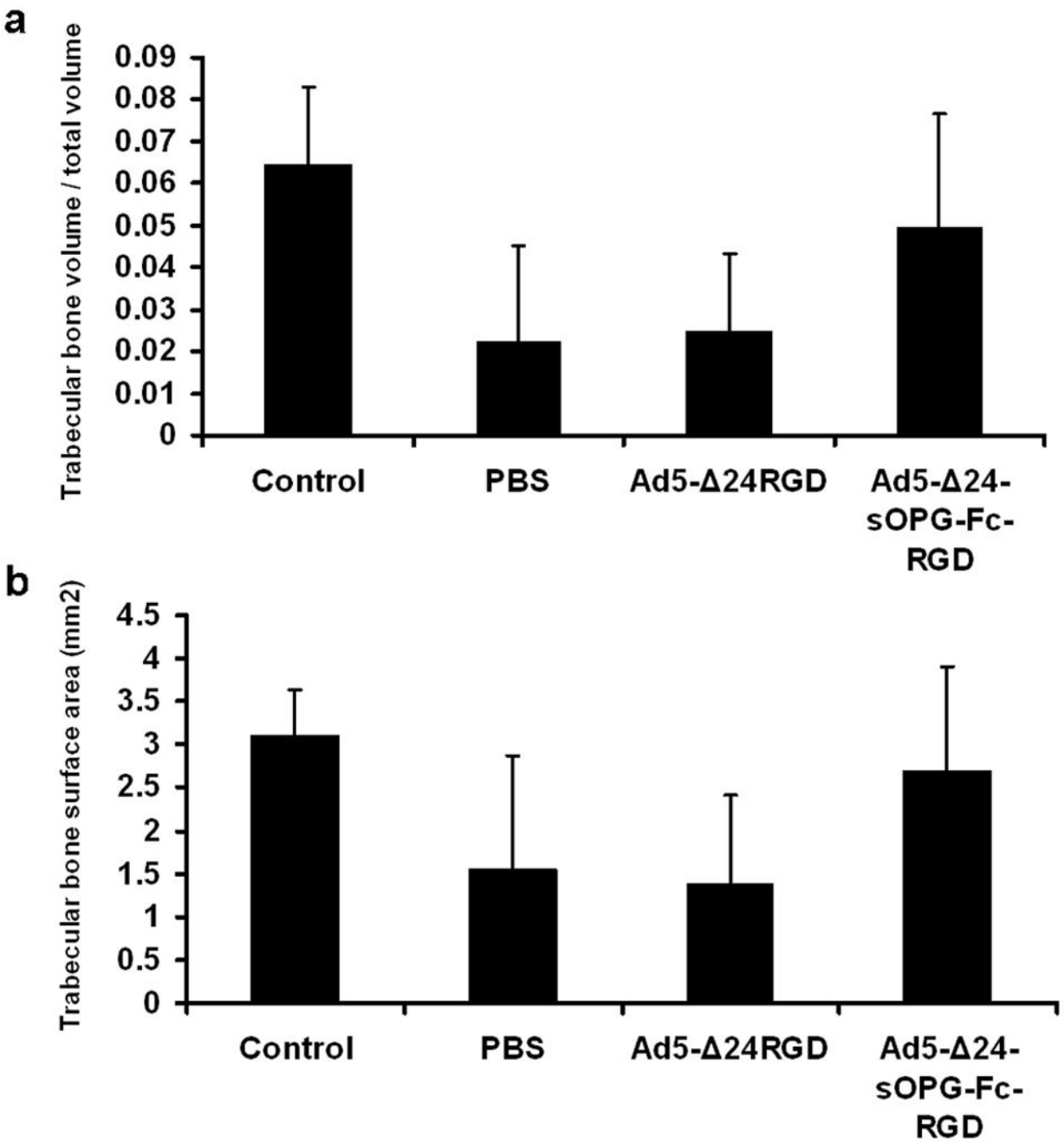

Fig. 6.

SCID mice bearing intratibial tumors of C4-2B-LUC were administered intratibial injections of Ad5-Δ24-sOPG-Fc-RGD, Ad5-Δ24RGD, PBS, or left untreated as controls. Tibiae were harvested at sacrifice and subjected to μCT. Analysis of μCT images was performed to determine the ratio of total volume to trabecular bone volume (*a*) and trabecular bone surface area (*b*). Shown are the group means ± SD, n = 3 (control), 6 (PBS), 7 (Ad-Δ24RGD) and 7 (Ad-Δ24-sOPG-Fc-RGD)